Chapter 6

H_2O_2 Hydroxylated rare earth ferrites ($LaFeO_3$ and $GdFeO_3$) Nanofillers in Poly (Vinylidene Fluoride) based Nanocomposite Films

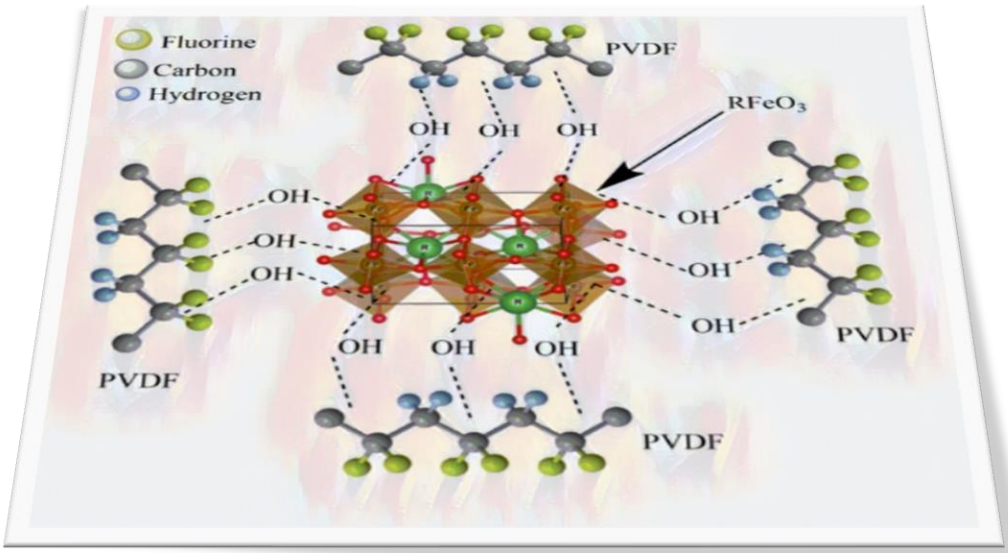

Chapter 6: H_2O_2 Hydroxylated rare earth ferrites ($LaFeO_3$ and $GdFeO_3$) Nanofillers in Poly (Vinylidene Fluoride) based Nanocomposite Films

8.1 Introduction

We have synthesized the nanocomposite films in the previous chapters have demonstrated the promising results. Keeping in the mind, we have done further literature review to understand the enhancement in the nanocomposite films. We come to know, that rare earth ferrites are semiconducting materials with the good dielectric constant as well in comparison to previous chosen filles in the Chapter 3 to 4. Thus, the rare earth ferrite could be better and promising fillers to enhance properties of the PVDF. Rana et al. have developed the flexible film PVDF/$LaFeO_3$ showing improved dielectric constant and at low range of electric field application for investigating polarization enhancement [129]. Samal et al. also used $BiFeO_3$ nanofiller in PVDF to develop nanocomposite film showing the highest enhanced value of dielectric constant (ε_r) = 16 with enhancement in the polarization [73]. Rare-earth orthoferrites ($RFeO_3$) are known to have semiconducting nature with small band gap, in addition to fascinating multiferroic properties [182]. Thus, they can offer additional functionality when used as filler in PVDF nanocomposites for energy storage applications. The particle size of multiferroic filler can play a crucial role during charge transport process at the interfaces. High energy ball milling method can be easily used to synthesize nanoparticles of these multiferroics [183]. In the present work, we have used high energy ball milling synthesis process to prepare $LaFeO_3$, $GdFeO_3$ nanoparticles and used them as filler in PVDF matrix to develop nanocomposites with better energy storage. We have optimized the vol% of the rare earth ferrites filler with the help of various theoretical nanocomposite mixing models based on the different theories. We have improved the dielectric constant and ferroelectric properties of PVDF with these fillers first time with the help of hydroxylation to the best of our knowledge.

8.2 Experimental

8.2.1 $GdFeO_3$, $LaFeO_3$ Nanoparticles Synthesis and Hydroxylation

The $GdFeO_3$, $LaFeO_3$ were prepared by using solid-state method with the help of high energy ball mill (PM400 MA, RETSCH, Gmbh, Germany). The reactants were mixed in stochiometric proportions in ethanol medium using zirconia balls at 300 rpm (rounds per minute) for 16 hrs. The ball-milled mixture was dried at 80℃ and calcined at 1000℃ to get nanocrystalline $LaFeO_3$ and $GdFeO_3$ ceramic powders. For hydroxylation of rare earth ferrite nanoparticles, the grinded ceramic powders were transferred to water solution of H_2O_2 (30% by volume), kept for 6 hrs at 105℃ and then dried at 120℃ for whole night.

8.2.2 Synthesis of Nanocomposite Film

Fabrication of PVDF nanocomposite films has been done by using solution cast method with DMF as the solvent. We took 10 % volume by volume of hydroxylated $LaFeO_3$ and $GdFeO_3$ to that of PVDF amount for preparation of nanocomposites. Filler nanoparticles were dispersed in 5ml DMF and ultrasonicated for 15 minutes followed by keeping it on the magnetic stirrer for 1 hr at 55℃ as shown schematically in **Figure 6.1**. Simultaneously, PVDF was dissolved in 10 ml DMF and stirred on the magnetic stirrer for 1 hour at 55℃. After 1 hr of stirring, both the precursors were mixed and kept for stirring for further 8 hrs at 55℃. With the evaporation of solvent, the mixed precursor became thick which was then ultrasonicated for 15 minutes. After sonication the viscous precursor was casted on a glass petri dish and kept for 120℃ for whole night. **Figure 6.1** illustrates the whole synthesis and fabrication process of PVDF/Hy-GdFO and PVDF/Hy-LFO nanocomposite films. The thickness of the films is measured to be 0.08±0.002mm.

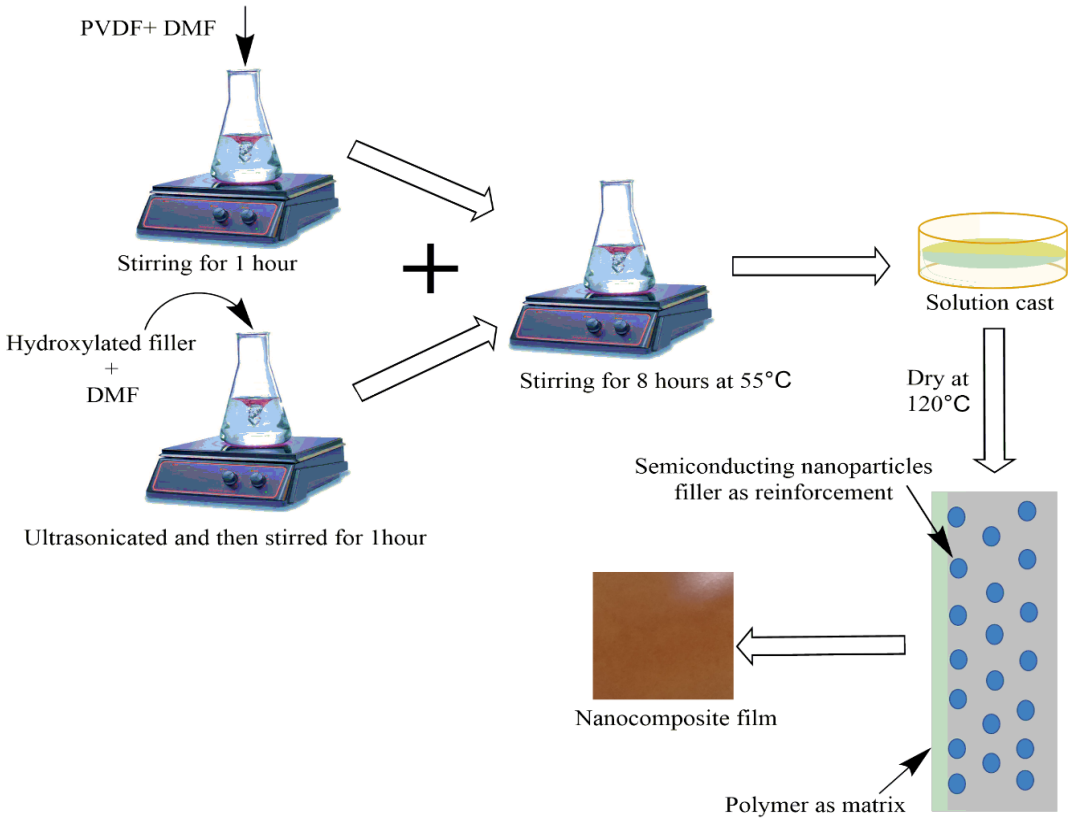

Figure 6.1 Synthesis of PVDF/Hy-GdFO and PVDF/Hy-LFO nanocomposite films.

8.3 Results and discussion

The schematic representation of 'rare earth ferrite filler' attachment to the PVDF polymer matrix facilitated by the hydroxylation is shown in **Figure 6.2**. The R in $RFeO_3$ represents the Gd and La. Hydroxylation of the ferrite nanoparticles actively modifies the surface, which make them more reactive to the PVDF, to provide better compatibility resulting into better nanocomposites with the PVDF matrix[184].

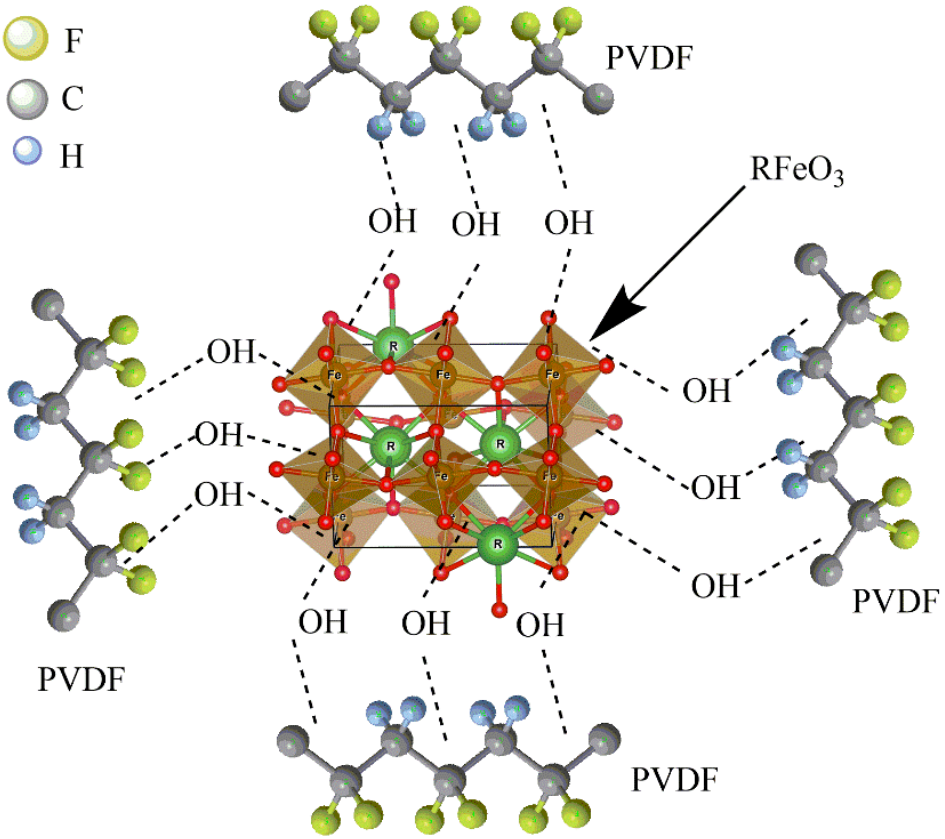

Figure 6.2 Schematic representation of PVDF-Filler bonding with the help of -OH.

8.3.1 Structural Analysis

The XRD patterns of calcined $LaFeO_3$, $GdFeO_3$ nanoparticles along with PVDF, PVDF/Hy-GdFO and PVDF/Hy-LFO nanocomposite films are shown in **Figure 6.3**. Indexing of the XRD patterns reveals pure perovskite phases of $LaFeO_3$, $GdFeO_3$ as all the XRD peaks match well with the JCPDS file 13-1493 for $LaFeO_3$ and 047-006 for $GdFeO_3$. Both the ferrites crystallize into single phase pure perovskite having orthorhombic crystal structure with *Pbnm* (equivalently *Pnma*) space group [26,185–189].

The XRD patterns of PVDF, PVDF/Hy-GdFO and PVDF/Hy-LFO nanocomposite films reveal three mixed phases α, β and γ. As can be seen in Fig.3, the β-phase is dominating along with the peaks of fillers in nanocomposite. The XRD peaks at 20.6º, 36.6º and 44.3º correspond to the β-phase, while peaks at 18.5º and 39.0º are from γ-phase[146,190,191]. The non-polar α-phase

XRD peaks are observed at 26.5º, 53.1º. The FTIR plots of $GdFeO_3$, $LaFeO_3$ are shown in **Figure 6.4(a)** while that for PVDF PVDF/Hy-GdFO and PVDF/Hy-LFO nanocomposite are shown in **Figure 6.4(b)**. In the FTIR of $LaFeO_3$ and $GdFeO_3$, stretching of Fe-O is observed at 559 cm^{-1} which shows the formation of perovskite structure of $LaFeO_3$, $GdFeO_3$. The absorbance peaks at 1386 cm^{-1} and 1659 cm^{-1} correspond to -OH group, that provide evidence of the hydroxylation of $GdFeO_3$ and $LaFeO_3$ nanoparticles with H_2O_2 [186,187,189,192]. The FTIR plot for pure PVDF shown in Figure 6.4(b) reveals that it is having all the three phases α, β, and γ, but β and γ-phases are in dominance. Absorption peaks corresponding to β-phase are observed at 510 cm^{-1}, 1071 cm^{-1}, 1274 cm^{-1} and 473 cm^{-1} and γ-phase at 840 cm^{-1}, 876 cm^{-1} and 1231 cm^{-1}. However, for α-phase, absorption peaks are noticed at 1400 cm^{-1} and 881 cm^{-1} [146,190,191]. As can be seen from **Figure 6.4(b)**, the peaks corresponding to β and γ-phases are prominent after nanocomposite formation as well.

The DSC measurement data for the pure PVDF and nanocomposite films are shown the **Figure 6.5**. In DSC plot, the endothermic peak at 167°C is corresponding to the melting of the β, and γ-phase for the pure PVDF and nanocomposite films [58,170]. In the DSC plot of PVDF, there is a small endothermic melting sign at 160.42°C, which correspond to the melting of α-phase. This feature is absent in the nanocomposite films [58,170], which suggest that incorporation of the fillers in PVDF nanocomposite significantly suppresses the formation of α-phase [30,31].

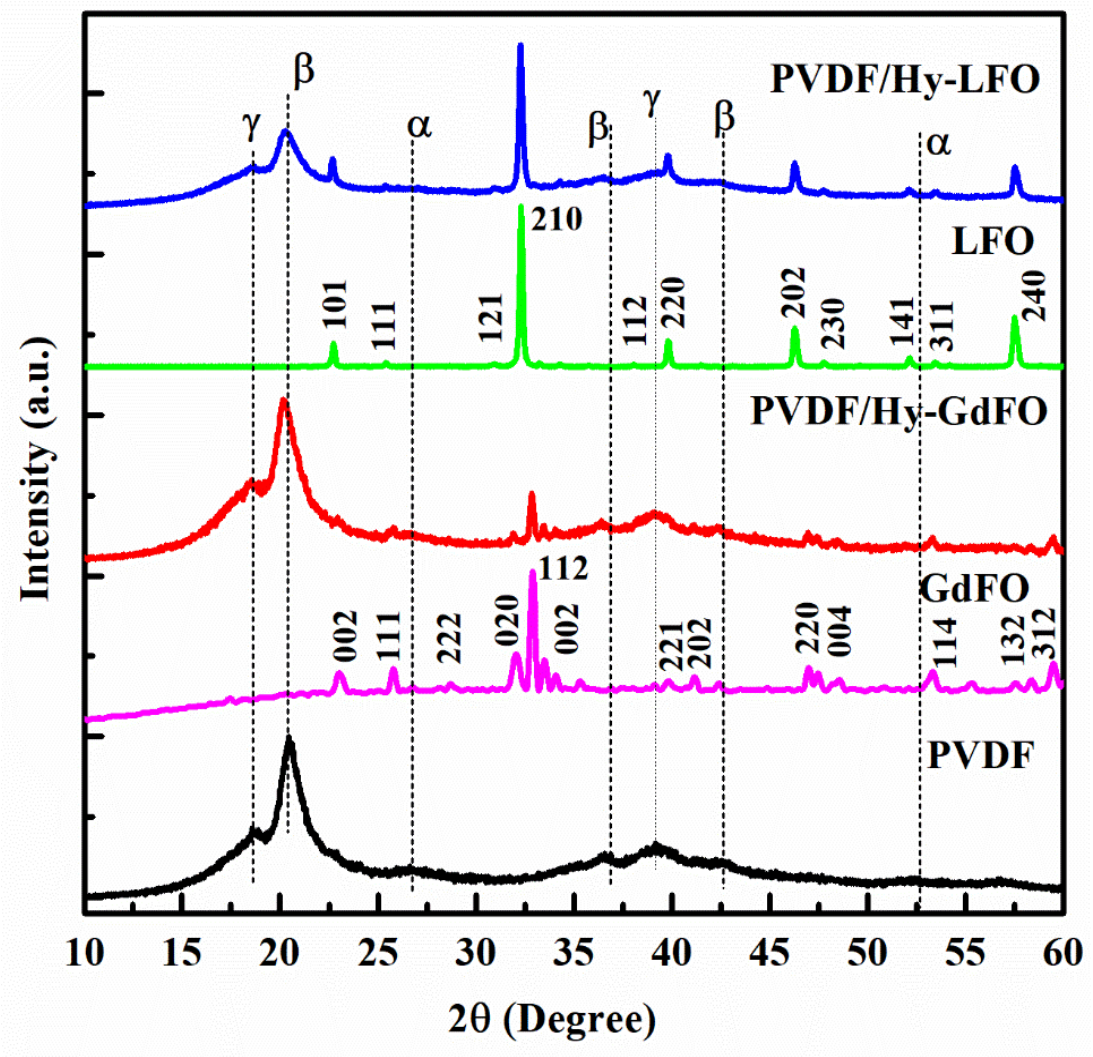

Figure 6.3 XRD patterns of PVDF, $GdFeO_3$ (GdFO), PVDF/Hy-GdFO, $LaFeO_3$ (LFO) and PVDF/Hy-LFO.

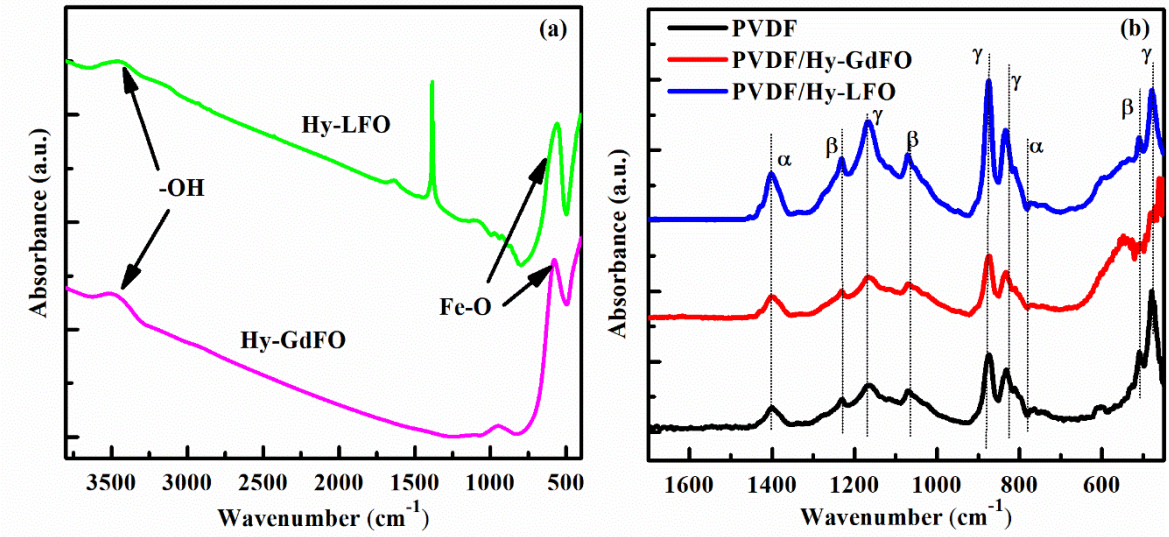

Figure 6.4 The FTIR spectra of (a) hydroxylated $LaFeO_3$ (Hy-LFO), hydroxylated $GdFeO_3$ (Hy-GdFO nanoparticles, and (b) PVDF and PVDF/Hy-LFO, PVDF/Hy-GdFO nanocomposite.

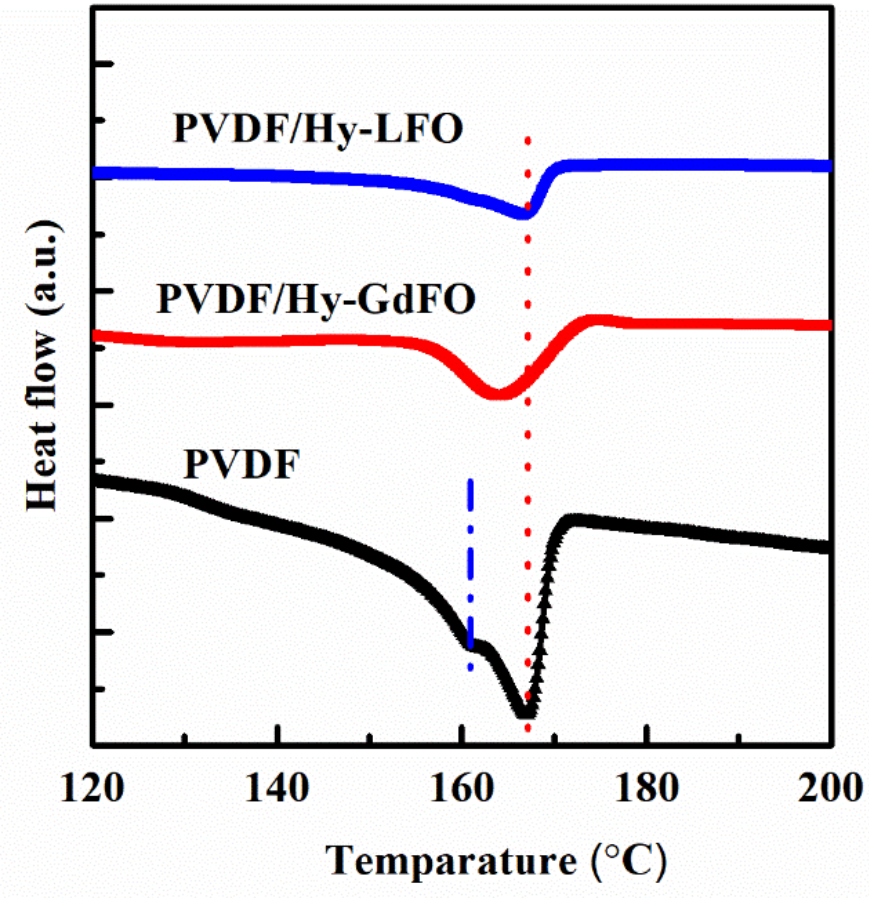

Figure 6.5 DSC plot for PVDF and PVDF/Hy-LFO, PVDF/Hy-GdFO nanocomposite films.

8.3.2 Morphological Analysis

The micrographs of the fillers are shown in the **Figure 6.6(a-b)** and size has been calculated with the help of ImageJ software and shown as histogram by gaussian fit. The **Figure 6.6(c-e)** shows the micrographs of PVDF and nanocomposite films taken with the help of 'Field emission gun' scanning electron microscope (FESEM).

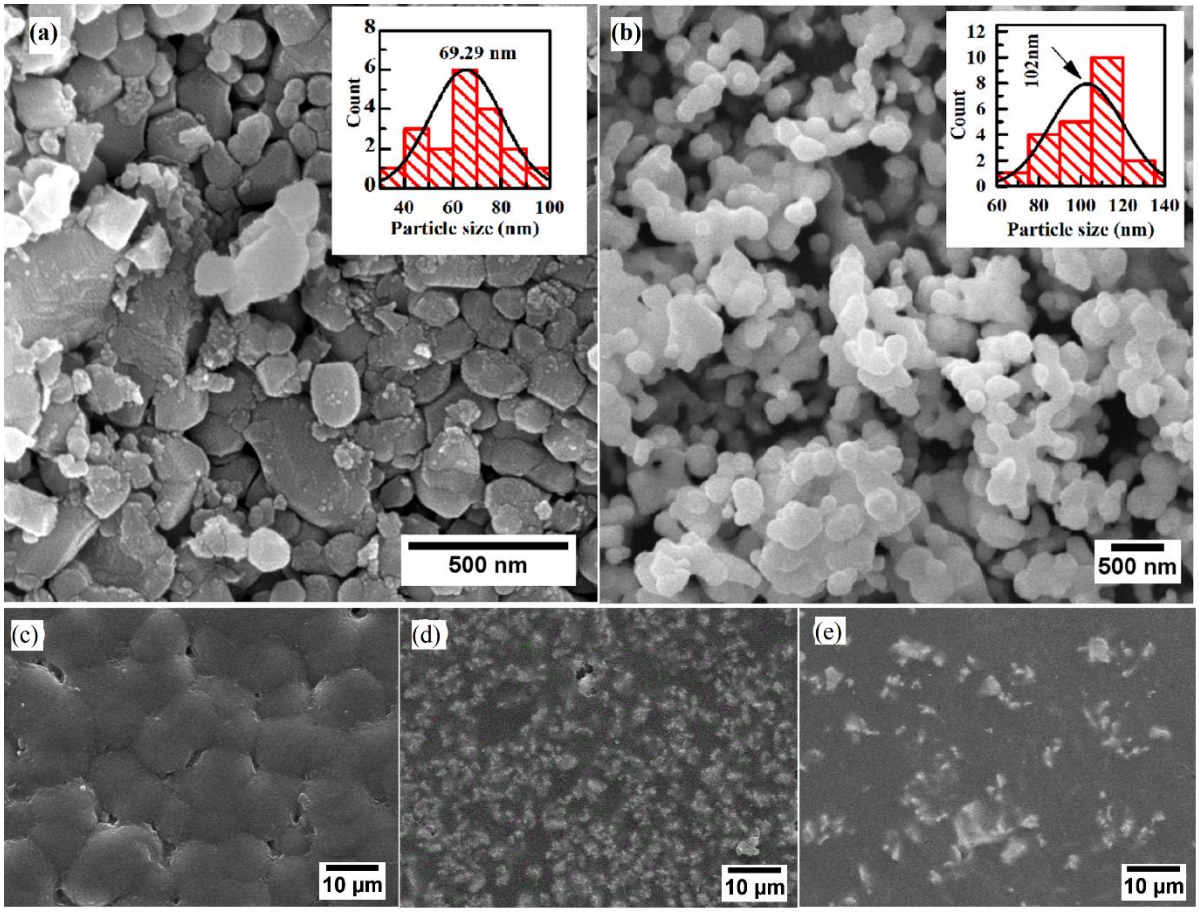

Figure 6.6 FESEM micrographs of (a) $LaFeO_3$ with histogram(inset), (b) $GdFeO_3$ with histogram (inset), (c) pure PVDF, (d) PVDF/Hy-GdFO and (e) PVDF/Hy-LFO Nanocomposite film.

The pure PVDF film is having spherulites with the approximate size of 12µm indicating the presence of crystallinity with nucleation and growth process in the film. As the Hydroxylated filler is loaded to the PVDF matrix, the spherulites can't be seen in the nanocomposite films as shown in the **Figure 6.6 (b-c)**, probably due to the reduction of spherulites size. The loading of 10 vol% of the filler in the matrix results in the reduction of the spherulite size because the nucleation process is much faster than the growth as the filler nanoparticle incorporated in PVDF matrix act as nucleation sites [111,152]. The smoother surface with no defects can be attributed to the fine arrays of the very tiny spherulite. The loaded filler is clearly observable in the nanocomposite films.

8.3.3 Dielectric and Ferroelectric Properties

Figs. 7(a-b) show the temperature dependent variation of dielectric constant (ε_r) and dielectric loss (tanδ) for PVDF, PVDF/Hy-GdFO and PVDF/Hy-LFO nanocomposite films, respectively, measured at a frequency of 1 kHz. At room temperature, the loading of 10vol% of Hy-LFO, Hy-GdFO in PVDF has significantly enhanced the dielectric constant for nanocomposite films (ε_r ~22 and ~15.15 respectively), that is much higher in comparison to pure PVDF (ε_r ~ 9) [68]. The dielectric loss also slightly increases with the loading of filler but it is in the acceptable range. As the temperature is increased, the dielectric constant of nanocomposite films increase abruptly due to increased mobility of the polar molecules [40,139]. This enhancement can be attributed to the β-phase dominance due to filler loading and interfacial interaction between the filler nanoparticles [33,34]. **Figure 6.7(c-d)** display frequency-dependent variation in dielectric constant (ε_r) and dielectric loss (tanδ), respectively, measured at room-temperature for PVDF, PVDF/Hy-GdFO and PVDF/Hy-LFO nanocomposite films. The dielectric constant decreases with increasing frequency as the measure contribution comes from the interfacial polarization[40,139] which reduces at higher frequencies. The interfacial space charge polarization is caused at the interfaces of heterogeneous systems [32-34]. The dielectric loss of the PVDF/Hy-LFO, PVDF/Hy-GdFO nanocomposites films is less than the PVDF films at higher frequency as can be seen in the **Figure 6.7 (d)**. The reason behind this could be that, when dielectric loss is measured in the low-frequency range, the loss is mostly due to conduction loss caused by leakage current in the interface polarization. The dielectric loss of nanocomposites at higher frequencies are mostly the relaxation polarization loss generated by the polarization of the material's dipole [34, 35]. The value of relaxation polarization dielectric loss is determined by the molecular interaction and the material's inherent relaxation state. At higher frequency, the dielectric loss of the nanocomposite films after loading filler in PVDF matrix is marginally lower than that of pure

PVDF because the relaxation states of filler nanoparticles and polymer matrix are notably different [193] as shown in the **Figure 6.7(d)**.

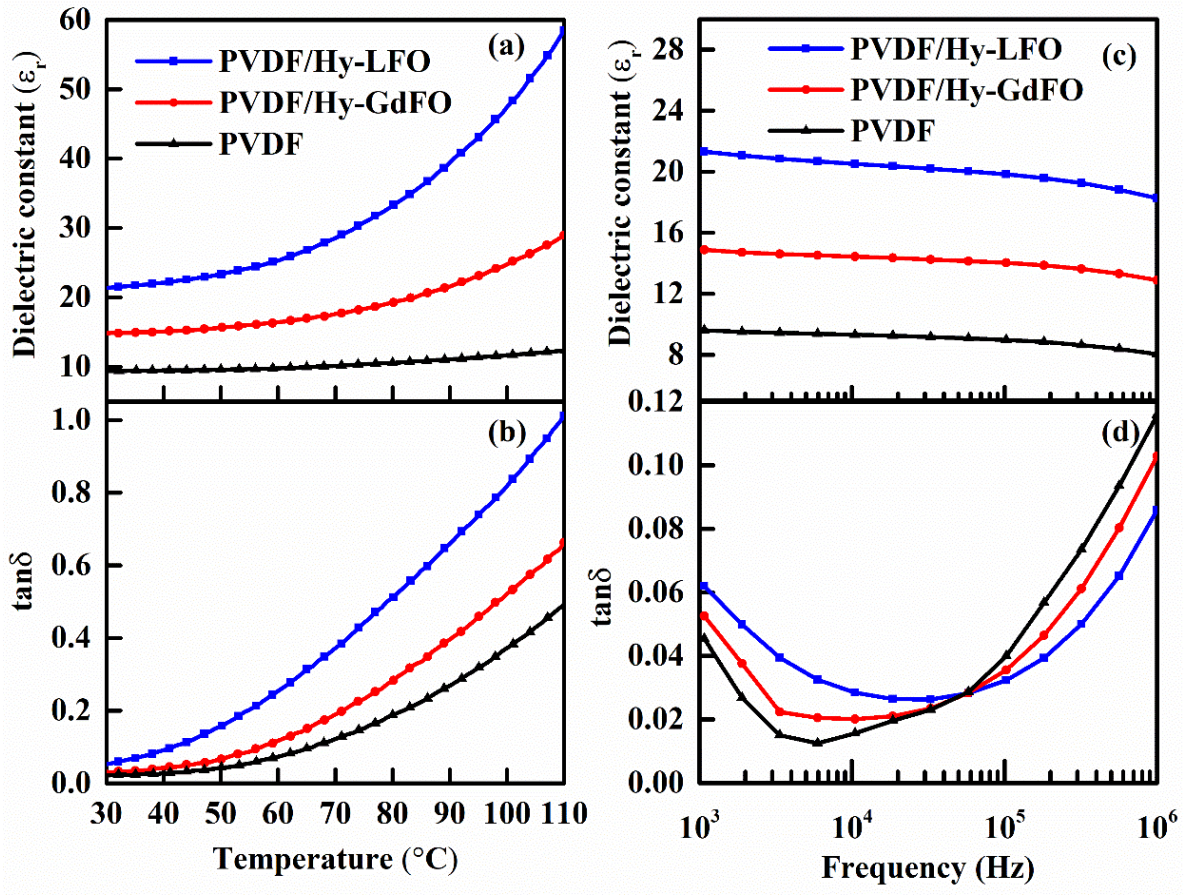

Figure 6.7 Temperature-dependent (a) dielectric constant, (b) dielectric loss; Frequency-dependent (c) dielectric constant and (d) dielectric loss; for pure PVDF and PVDF/Hy-LFO, PVDF/Hy-GdFO nanocomposite films measured at 1 kHz.

In **Figure 6.8(a-b)**, the histogram shows the difference in the values of dielectric constant and dielectric loss at 30ºC and 100ºC temperatures for pure PVDF, PVDF/Hy-GdFO and PVDF/Hy-LFO nanocomposite films. It demonstrates that the nanocomposite formation significantly improves the dielectric properties of PVDF at room temperature as well as at higher temperatures. To understand the temperature and frequency dependence of the dielectric properties in more detail, **Figure 6.9(a-f)** shows the dielectric plots for all the films measured at various frequencies with varying temperature. The nature of variation of dielectric constant

with temperature for pure PVDF and its nanocomposites is similar at all frequencies. The decrement in dielectric constant with the increasing frequency is due to the decrement in the number of dipoles aligned in the direction of applied electric field [179,194,195]. As the temperature is increasing, the dielectric constant for all the films shows increasing trend. This can be attributed to the improvement in the segmental motion of the molecular chains of PVDF matrix that are frozen at lower temperature.

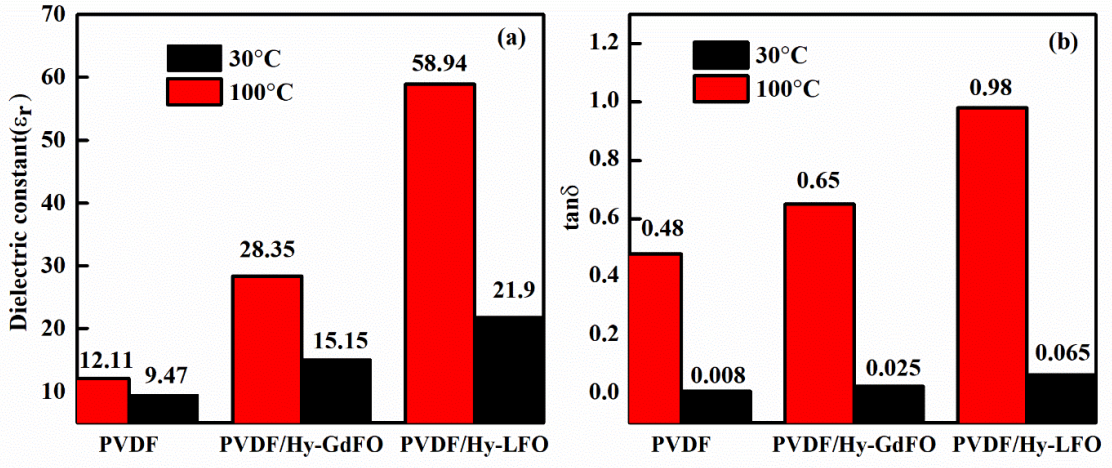

Figure 6.8 Comparison of dielectric constant and dielectric loss at 30℃ (black columns) and 100℃ (red columns) for pure PVDF; PVDF/Hy-GdFO and PVDF/Hy-LFO nanocomposite films.

The nanocomposite films exhibit higher dielectric constant which is due to the Maxwell-Wagner-Sillars type interfacial and space charge polarization as the loading of the nanofiller enables the formation of micro capacitors in the films as shown schematically in **Figure 6.10** The loading of filler also generates higher number of free charge carriers [179,194–197].

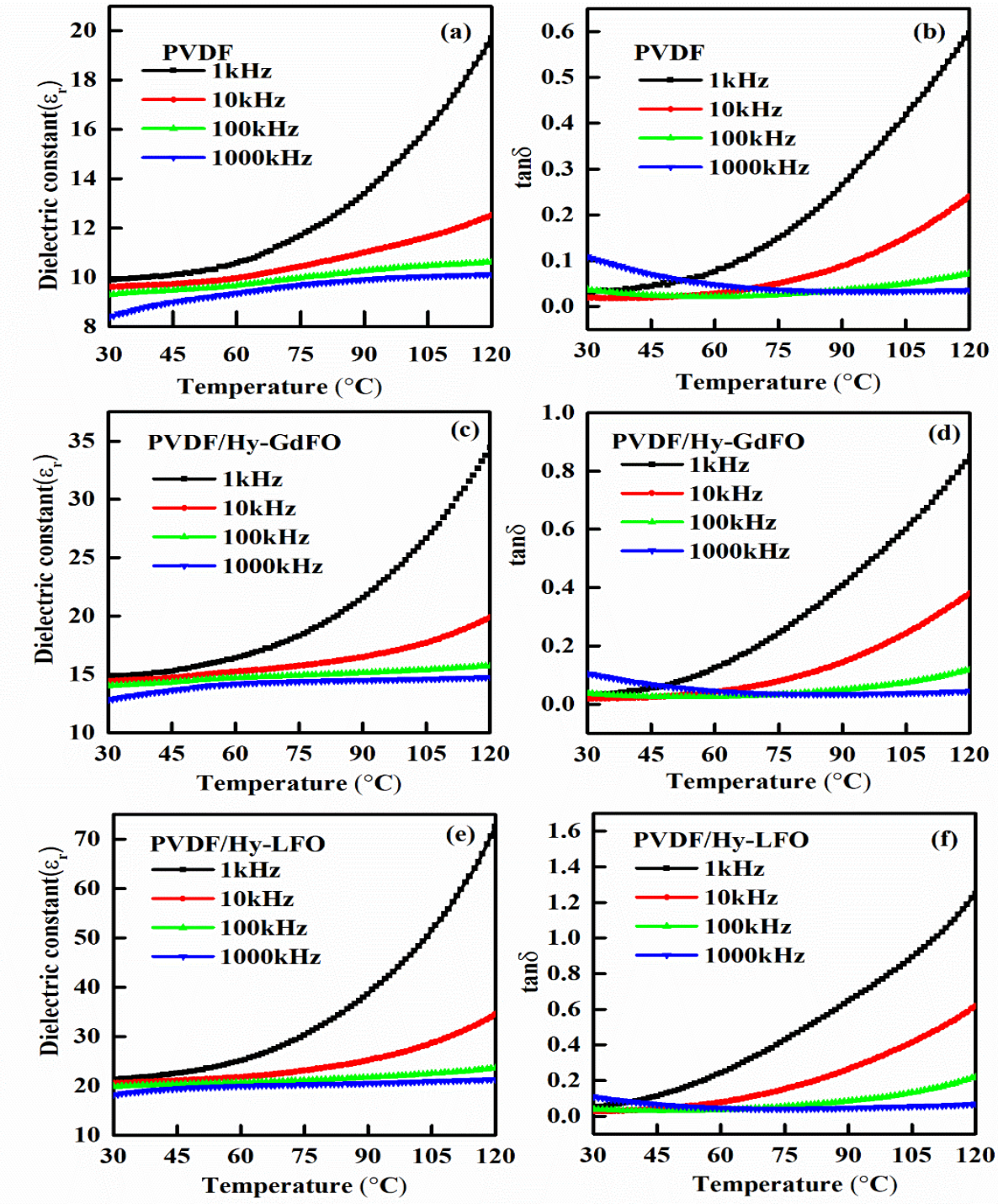

Figure 6.9 Temperature dependence of dielectric constant and loss for PVDF, PVDF/Hy-GdFO, PVDF/Hy-LFO films measured at various frequencies.

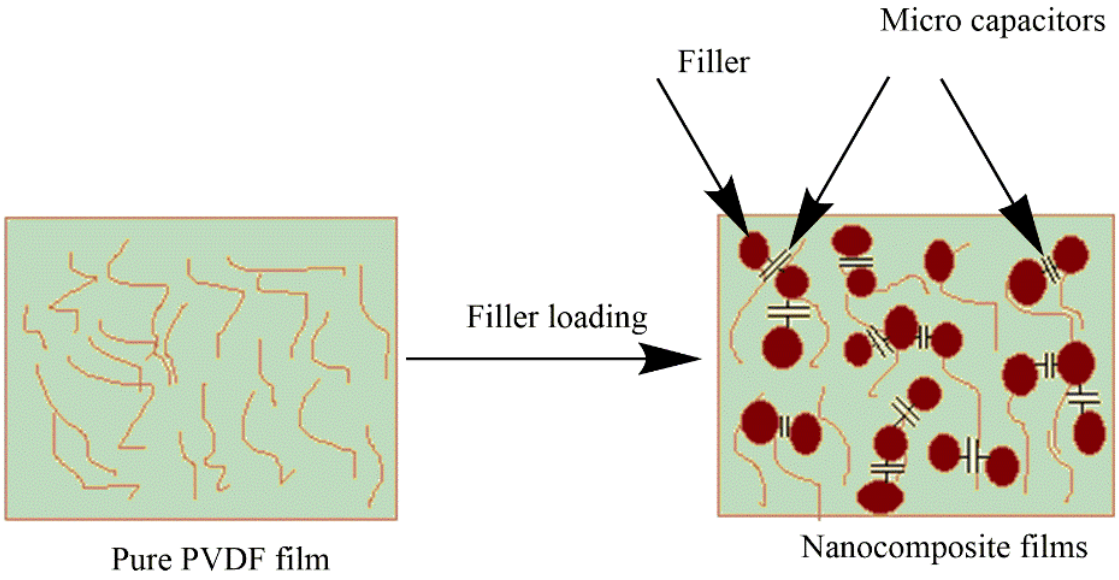

Figure 6.10 Schematic diagram illustrating the formation of micro-capacitors in the nanocomposite due to loading of the filler.

Temperature dependence of dielectric constant and loss of the rare earth ferrite nanofillers measured on pellets sintered at 1300^{o}C are shown in the **Figure 6.11(a)**. The $GdFeO_3$ has significantly higher dielectric constant in comparison to $LaFeO_3$ but the loss for the $GdFeO_3$ is also prominent especially above 60^{o}C. To verify that which model of interfacial and space charge polarization contributions are effective in the nanocomposite films, we have theoretically calculated the dielectric constant of nanocomposites using various models reported in the literature [43-45].

Different equations to predict the dielectric constant of nanocomposites have been proposed in the literature as given below:

Bruggeman model [15]

$$\emptyset_c \left(\frac{\varepsilon_c - \varepsilon_{eff}}{\varepsilon_c + 2\varepsilon_{eff}}\right) + \emptyset_p \left(\frac{\varepsilon_p - \varepsilon_{eff}}{\varepsilon_p + 2\varepsilon_{eff}}\right) = 0. \qquad (6.1)$$

Jayasundere-Smith model [198]

$$\varepsilon_{eff} = \frac{\emptyset_p \varepsilon_p + \emptyset_c \varepsilon_c [3\varepsilon_p/(\varepsilon_c+2\varepsilon_p)][1+3\emptyset_c(\varepsilon_c - \varepsilon_p)/(\varepsilon_c+2\varepsilon_p)]}{\emptyset_p + \emptyset_c [3\varepsilon_p/(\varepsilon_c+2\varepsilon_p)][1+3\emptyset_c(\varepsilon_c - \varepsilon_p)/(\varepsilon_c+2\varepsilon_p)]}. \quad (6.2)$$

Maxwell-Garnett model[199]

$$\varepsilon_{eff} = \varepsilon_p \left[1 + \frac{3\emptyset_c(\varepsilon_c - \varepsilon_p)}{3\varepsilon_p - \emptyset_c(\varepsilon_c - \varepsilon_p)}\right]. \quad (6.3)$$

Where ε_{eff}, ε_c, and ε_p denote the nanocomposite's effective dielectric constants and the effective dielectric constants of the ceramic filler, and polymer matrix, respectively. The volume fractions of filler and matrix are represented as $\emptyset_c$, $\emptyset_p$ respectively.

The dielectric constant values calculated by the three predicted theoretical models are shown in **Figure 6.11(b)** for comparison. The experimental results are close to the prediction from the Bruggeman model. Since the fine details of the interfacial effects are not taken into the consideration in the calculation, that can be the reason for the gap between theoretically predicted and experimentally measured values [101].

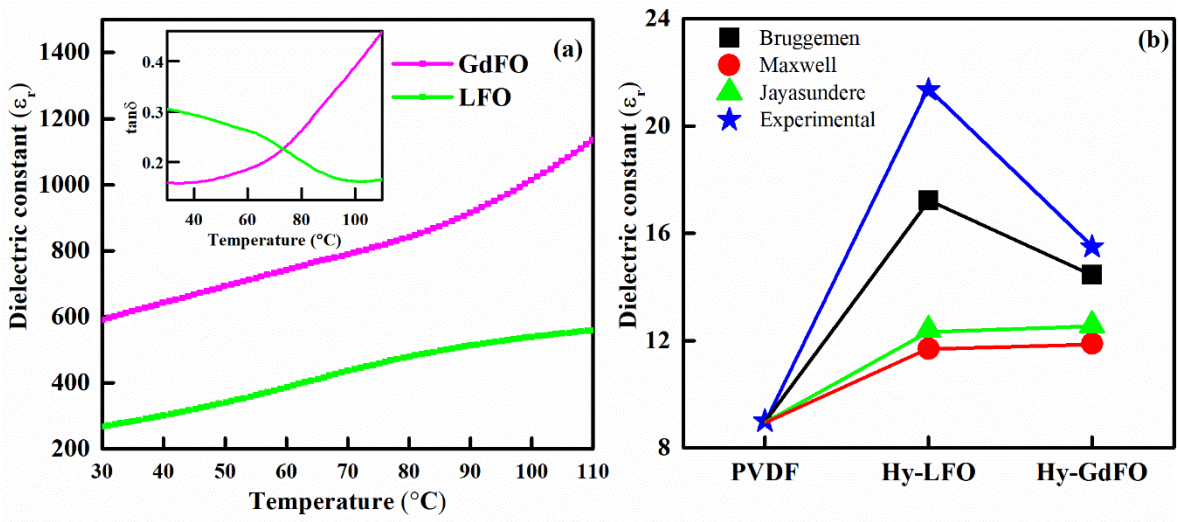

Figure 6.11 (a) Dielectric constant and loss (inset) of the ferrite fillers, (b) Comparison of theoretical models and experimental data.

The AC conductivity of pure PVDF and its nanocomposites is calculated using the expression $\sigma = 2\pi f\, \varepsilon_0\, \varepsilon_r \tan\delta$; where σ is AC conductivity, f is frequency and ε_0 is the

permittivity of space [164] and the plots are shown in **Figure 6.12(a-b).** The nature of conductivity plots is similar for all the films. As the temperature and frequency increases the conductivity also increases. The increment in the conductivity with frequency is following the power law ($\sigma \propto \omega^s$) with exponent between 0-2, as determined from the slope of the graph [164]. In the conductivity expression, there is ε_r which dominates the trend of plots instead of tanδ as the value of ε_r for the ferrite nanocomposite films is much higher than pure PVDF.

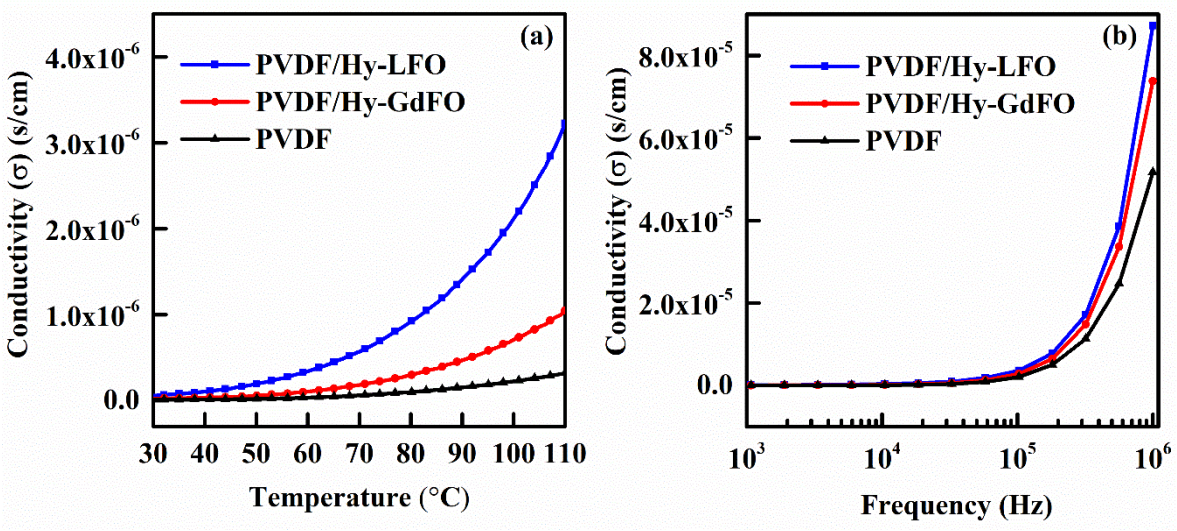

Figure 6.12 (a) AC conductivity vs temperature measured at 1kHz and (b) AC conductivity vs frequency at room temperature, for PVDF and nanocomposite films.

Polarization (P) versus electric field (E) hysteresis loops of PVDF, PVDF/Hy-LFO and PVDF/Hy-GdFO nanocomposite films measured at 20Hz frequency, and 800kV/cm electric field, are shown in **Figure 6.13(a)**. It can be seen that PVDF/Hy-LFO and PVDF/Hy-GdFO nanocomposites have better polarization as comparison to pure PVDF. The enhancement in the polarization of nanocomposites is caused by the interfacial space charge polarization due to the filler loading in the PVDF matrix [31-32]. The values of maximum and remanent polarization are listed in the table 1 for these samples. Further, we have calculated the energy density and energy discharging efficiency for the nanocomposite films with the help of equations (1.11) and (1.13) below:

$$\text{Energy storage density } (U_d) = \int_{P_r}^{P_{max}} E dp \quad (1.11)$$

$$\text{efficiency } (\eta\%) = \frac{U_d}{U_d + U_l} \times 100 \quad (1.13)$$

where U_d and U_l are energy storage density and energy loss density, respectively, and P_r is the remnant polarization, E is the applied electric field and P_{max} is the maximum polarization with respect to maximum experimental electrical field [134,200].

Table 6.1. Values of maximum polarization and remanent polarization for PVDF and nanocomposite films determined from P-E loops at 800kV/cm applied electric field at 20Hz.

Sample	P_r (μC/cm^2)	P_{max} (μC/cm^2)
Pure PVDF	0.05	0.63
PVDF/Hy-GdFO	0.16	0.97
PVDF/Hy-LFO	0.26	1.01

Both the nanocomposite films have better energy density than pure PVDF. A comparison of our results with the previous reports on similar systems is given in Table 2. The dielectric constant and energy storage density for our samples is significantly better than the PVDF-$BiFeO_3$ based nanocomposite. Thus, nanocomposites developed in present work have significant promise for energy storage applications. **Figure 6.13(b)** demonstrates the energy density and energy discharging efficiency for pure PVDF and PVDF/Hy-LFO, PVDF/Hy-GdFO nanocomposite films. The energy discharging efficiency for the PVDF/Hy-GdFO nanocomposite film is found to be 66.37 %, which is quite good with better energy density.

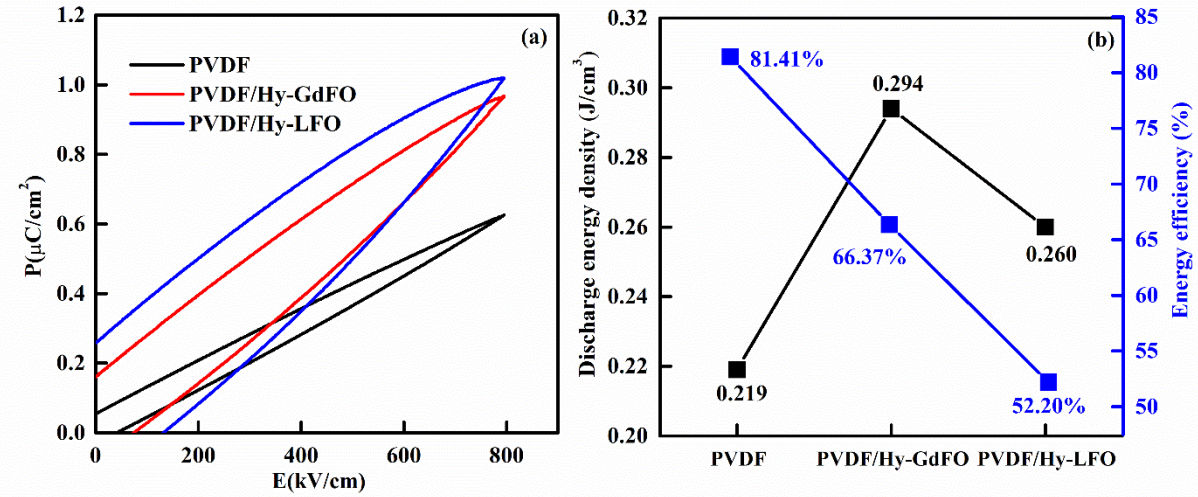

Figure 6.13 (a) P-E hysteresis loop of PVDF, PVDF/Hy-LFO and PVDF/Hy-GdFO nanocomposite films and (b) Energy density and energy discharge efficiency.

Table 6.2. Comparison of energy density and dielectric constant with previously reported work.

Sample	Energy Density (J/cm^3)	ε_r	Reference
PVDF/Hydroxylated $GdFeO_3$	0.294	~15.15	This work
PVDF/Hydroxylated $LaFeO_3$	0.260	~22	This work
rGO-Ag/PVDF	0.26	-	[49]
PVDF/ Hydroxylated $BiFeO_3$	0.14515	~15	[17]

The breakdown strength test was also done on the PVDF, PVDF/Hy-GdFO and PVDF/Hy-LFO with the help of AC breakdown strength test set-up. We performed the seven breakdown tests on every film and then used the Weibull distribution given by equation (1.17) below [201,202].

$$P(E) = 1 - \exp\left[-\left(\frac{E}{E_b}\right)^{\beta}\right] \quad (1.17)$$

where *P(E)* is the cumulative prospect of electrical breakdown, E is the actual breakdown field, E_b is the breakdown field when the cumulative prospect is 63.2%, and β is the Weibull modulus (shape parameter) obtained by linear fitting, higher β represents the better results. We have drawn the plots between the two parameters Xi, Yi which are given by the equations (1.18) and (1.19) given below.

$$X_i = \ln (E_i)$$

$$Y_i = \ln \left[-\ln\left(1 - \frac{i}{n+1}\right)\right]$$

Where, $p(E) = \frac{i}{n+1}$, i is the consecutive number of samples for 'n' numbers of samples [101]. The Weibull distribution analysis is plotted in **Figure 6.14**(a). **Figure 6.14**(b) shows the breakdown strength and value of shape parameter (β) for the nanocomposite and pure PVDF films. Due to 10 vol% loading of the filler, more conducting paths are expected to appear while applying electric field which reduces the breakdown strength of the nanocomposites. Even though the breakdown strength has decreased for the nanocomposite films but it is still much better making them well suitable for the energy storage applications.

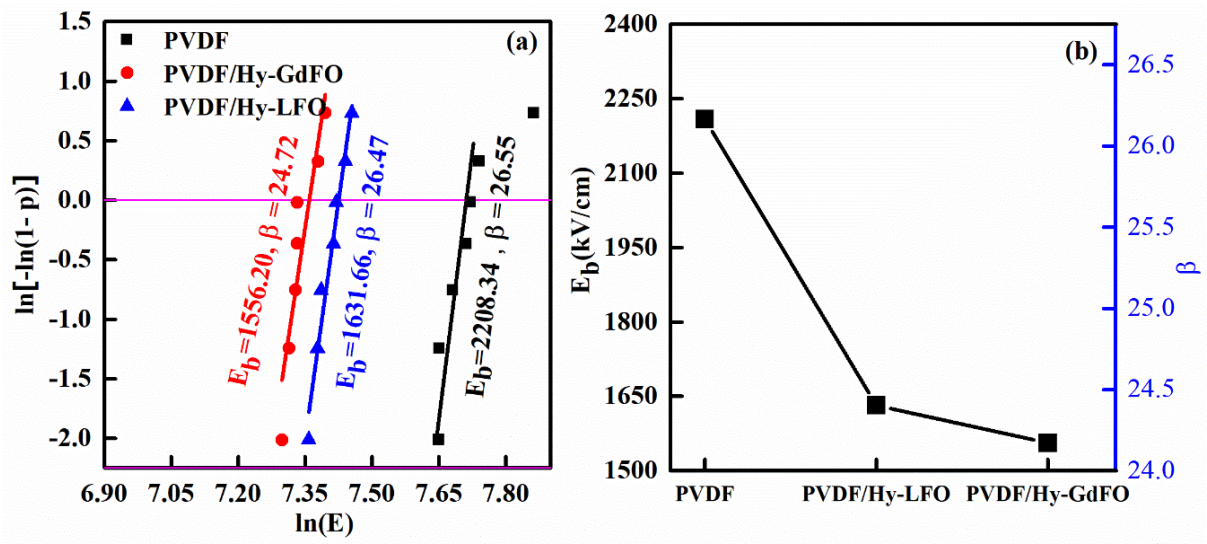

Figure 6.14 (a) Weibull Analysis of breakdown strength and (b) Comparison of breakdown strength and shape parameter (β) for PVDF and ferrite nanocomposite films.

8.4 Conclusions

we have successfully synthesized the orthorhombic $LaFeO_3$ and $GdFeO_3$ nanoparticles via high energy ball mill. The FESEM images confirm the size of rare earth ferrites with help of histogram with gaussian fit. The facile solution cast method has been employed for the preparation of polyvinylidene fluoride and rare earth ferrite nanocomposite films. The morphological analyses with the help of FESEM shows the smooth and defect free films and no spherulites can be seen in the films. FTIR shows the hydroxylation of ferrite fillers. Analyses of XRD and FTIR confirm the formation of polar phases (β, γ-phase) in dominance. The DSC measurements confirms the suppression of α-phase in nanocomposite films. At higher temperature nanocomposites have better dielectric properties (ε_r = ~58) in comparison of pure PVDF. The three theoretical models have been compared with the experimental values for dielectric properties. The dielectric constant (ε_r ~22) and ferroelectric properties (P_m = 1.01μC/cm^2) have been improved for the nanocomposite with the help of loaded hydroxylated $LaFeO_3$ filler and with $GdFeO_3$, we have got better energy density 0.294 J/cm^3 and Discharge energy efficiency found to be around 66.37 %.